Earth Planet. Sci. Lett. 626 (2024) 118522

Contents lists available at ScienceDirect

Earth and Planetary Science Letters

journal homepage: www.elsevier.com/locate/epsl

Periodic Bedrock Ridges at Oxia Planum and Chryse Planitia, Mars: Evidence for widespread aeolian erosion of an ancient surface by regional paleowinds

Elena A. Favaro [a,*], Matthew R. Balme [a], Joseph D. McNeil [a,b], Peter Fawdon [a], Joel M. Davis [c], Peter M. Grindrod [b], Stephen R. Lewis [a]

[a] School of Physical Sciences, The Open University, Milton Keynes, Buckinghamshire MK7 7EA, UK
[b] Department of Earth Sciences, Natural History Museum, London SW7 5BD, UK
[c] Earth Science & Engineering, Imperial College London, London SW7 2BX, UK

ARTICLE INFO

Edited by: Dr. F. Moynier

Keywords:
Periodic bedrock ridges
Oxia Planum
Fe/Mg-rich phyllosilicates
Mars global circulation model
ExoMars
Mars

ABSTRACT

Periodic Bedrock Ridges (PBRs) are repeating, symmetrical, wind-transverse, bedrock-abraded linear ridges that occur on Mars as parallel sets. Here, we extend our previous survey of PBRs at Oxia Planum – the landing site of ESA's ExoMars Rosalind Franklin rover – to include three additional sites along the margins of the circum-Chryse basin to understand patterns in PBR orientation and occurrence. We analyzed PBR crestline orientation at each study site and found them to be consistent across this large region, but their orientations do not align with global circulation model winds, suggesting contemporary winds are not responsible for PBR development. Furthermore, we used observations of landscape-level stratigraphic relationships at Oxia Planum to constrain the formation age of PBRs to be late Noachian to early Amazonian. Their consistent orientations and age suggest that the Chryse-margin PBRs formed concurrently and represent modification of an ancient palaeosurface. In addition, we find a tendency for PBRs to preferentially occur in regions where Fe/Mg-rich phyllosilicate minerals were detected in hyperspectral remote sensing data. We conclude that regional scale aeolian processes formed the circum-Chryse PBRs, and that exposed bedrock with Fe/Mg-rich phyllosilicate detections were either more susceptible to PBR formation, or better preserve PBRs than other regional lithologies.

1. Introduction

The surface of Mars bears extensive evidence of both aqueous and aeolian activity. At Oxia Planum, the landing site of ESA's *Rosalind Franklin* Rover (ERFR), both signals are imprinted on the landscape as fluvial valley networks and inverted channels (Fawdon et al., 2021, Fawdon et al., 2022; Davis et al., 2023), sediment fans (Quantin-Nataf et al., 2021), extensive Noachian-aged clay-bearing terrain (Carter et al., 2015; Carter et al., 2016; Carter et al., 2023; Mandon et al., 2021; Quantin-Nataf et al., 2021), and transverse aeolian ridges (TARs), wind streaks, dust devils, sand sheets, and periodic bedrock ridges (PBRs; Favaro et al., 2021; Silvestro et al., 2021). Interpreting these signals is critical to the nominal mission for both *ERFR* operations and in the search for evidence of ancient life preserved in biomarkers in the surface and subsurface of Oxia Planum; biomarker preservation depends partly on erosion rates (mainly by wind action) and length of time surfaces are exposed to the martian environment.

PBRs are abundant at Oxia Planum (Favaro et al., 2021; Silvestro et al., 2021), and are found throughout the circum-Chryse region. PBRs are wind-transverse meter- to decameter-scale repeating, symmetrical, linear ridges interpreted to have been carved directly into bedrock by transverse winds (Fig. 1b and c; Montgomery et al., 2012; Hugenholtz et al., 2015). Although several different models have been proposed for their formation (e.g. Montgomery et al., 2012; Hugenholtz et al., 2015; Stack et al., 2022), only that of Hugenholtz et al. (2015) is supported by field analogue observations on Earth. According to the Hugenholtz et al. (2015) model, PBRs form when sediment cover over bedrock self-organizes into megaripples (ripples with a bi- or multimodal grainsize distribution). As megaripples develop, larger (and possibly denser) clasts collect at the crestline through reptation, creep, and collision by saltating particles (Yizhaq et al., 2012; Hugenholtz et al., 2015), armoring finer grains beneath. Abrasion of the underlying

* Corresponding author.
E-mail address: elena.favaro@open.ac.uk (E.A. Favaro).

https://doi.org/10.1016/j.epsl.2023.118522
Received 7 July 2023; Received in revised form 25 October 2023; Accepted 28 November 2023
Available online 12 December 2023

bedrock surface begins in the troughs and lee (downwind) slopes where it is exposed, forming incipient PBRs (Hugenholtz et al., 2015). As the megaripple pulls away from the incipient PBR and migrates downwind, more of the underlying bedrock is exposed and abraded. Because PBRs are interpreted as wind-transverse landforms, they encode important climatic signals that can be used to reconstruct past wind regimes.

The OMEGA (Observatoire pour la Minéralogie, l'Eau, les Glaces et l'Activité; Bibring et al., 2004) instrument onboard ESA's Mars Express orbiter detected occurrences of hydrated minerals, including phyllosilicates, across the martian surface through visible and near-infrared spectroscopy (Bibring et al., 2006). Carter et al. (2023) produced high-resolution global maps showing the distribution and mineralogy of hydrated phases by combining the analysis of OMEGA data with that of CRISM (Compact Reconnaissance Imaging Spectrometer for Mars; Murchie et al., 2007). In the circum-Chryse basin, specifically (from Kasei Valles in the west, to Mawrth Vallis in the east, and Aram Chaos in the south; Fig. 1), the spectra of Fe/Mg-rich phyllosilicates most closely resemble those of Fe/Mg smectites (e.g. nontronite and saponite) or vermiculite clay minerals (Loizeau et al., 2007; Quantin-Nataf et al., 2021; Mandon et al., 2021; Brossier et al., 2022; Carter et al., 2023).

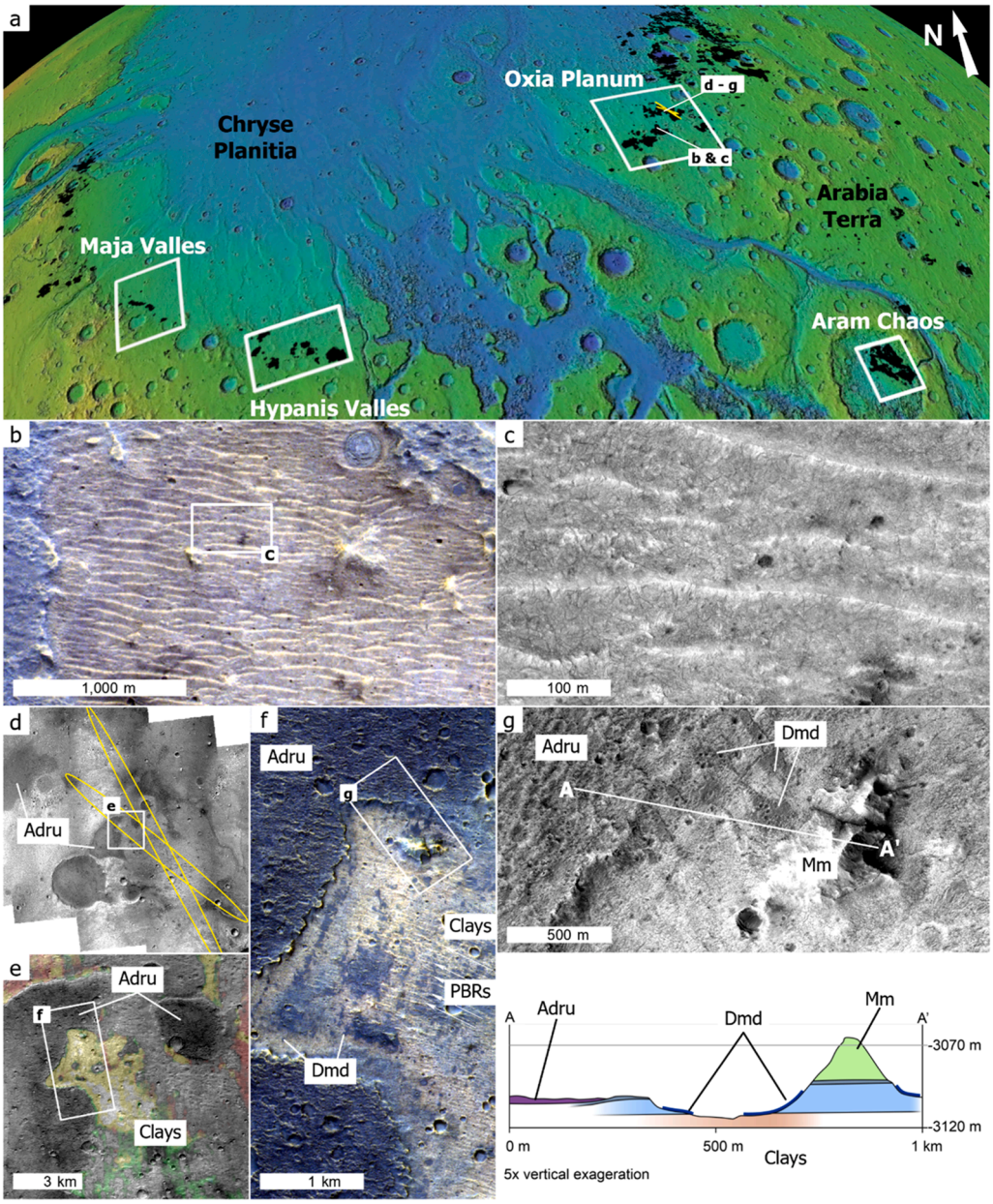

Fig. 1. (a) Location of Maja Vallis, Hypanis Valles, Aram Chaos, and Oxia Planum study areas including landing ellipses (yellow) for the ExoMars rover mission. Black patches denote detections of Fe/Mg-rich phyllosilicate minerals from a global catalogue of OMEGA data (Carter et al., 2023). (b) Examples of PBRs commonly observed in the orange-toned regions of CaSSIS Near Pan and Blue (NPB) data which is indicative of phyllosilicate-bearing materials (CaSSIS image MY36_016394_162_0). (c) The same bright ridges as seen in HiRISE (HiRISE image ESP_072518_1975) where fractures crosscutting the ridges indicate that they are part of the bedrock rather than superficial features. (d) Examples of the Adru appearing dark in the CTX data. (e) Adru is anti-correlated with phyllosilicate spectral signatures in CRISM (image no. R=BD1000, G=BD2400 B=BD1900). Yellow, green and orange show phyllosilicate signatures. (f) CaSSIS NPB (CaSSIS image MY37_023336_163_0) showing Adru in dark blue, phyllosilicate-bearing terrain in orange tones and the Dmd in blue-grey. The detailed relationships between these units, and others in the local stratigraphy (Quantin-Nataf et al., 2021; Fawdon et al., 2021; McNeil et al., 2022) are seen in (g) HiRISE (PSP_009735_1985) and in cross-section illustrating how the Adru overlies phyllosilicate-bearing terrains and the surficial Dmd post-dates all other units. Elevation data for the Cros-section available from (Volat et al., 2022).

High fidelity geologic mapping of the Martian surface has only been undertaken in a handful of areas, mostly coinciding with the landing sites of rovers and landers. While Oxia Planum has been the subject of fine-scale mapping ahead of the nominal *ERFR* mission (Fawdon et al., 2023a, b), the wider Chryse basin has only been described by Tanaka et al. (2014) and is therefore devoid of regional geologic interpretation. Here, we briefly summarize the geology of Oxia Planum, characterizing only a small fraction of a much larger region.

Oxia Planum is located on an extensive early Noachian (~4 Ga) layered, fractured clay-bearing basement (Quantin-Nataf et al., 2021; Mandon et al., 2021). The clay-bearing unit is made up of two subunits, identified and described in detail by Quantin-Nataf et al. (2021), and summarized here: a ~15 m thick upper unit characterized by decameter-scale fracture patterns, and a lower unit characterized by meter-scale closely spaced fractures. In High Resolution Imaging Science Experiment (HiRISE; McEwen et al., 2007) NIR-RED-BG images, these subunits have bluish and reddish hues, respectively. In Colour and Stereo Surface Imaging System (CaSSIS; Thomas et al., 2017) NIR-PAN-BLU images, areas with phyllosilicate detections present as orange and blue hues (Mandon et al., 2021; Bowen et al., 2022).

Two additional units of interest discontinuously overlie the clay-bearing terrain at Oxia Planum: The Amazonian dark resistant unit (Adru), and dark mantling deposits (Dmd). The Adru (Fig. 1d–g) is dark-toned and appears dark blue in CTX and CaSSIS images. Its rugged surface has retained small craters relative to the adjacent light-toned phyllosilicate-bearing terrain. The Adru has been dated to ~2.6 Ga, ranges in thickness from <1 m up to possibly 20 m thick and is located at the top of local stratigraphy. It is hypothesized to have formed by fluvial processes infilling now inverted topography, or as a volcanic deposit (Quantin-Nataf et al., 2021; Fawdon et al., 2022). Initial observation of this unit are described in Quantin-Nataf et al. (2021). The Dmd (Fig. 1f–h) comprises small (<500 m) patches of dark material distributed throughout Oxia Planum. Some examples appear to have a weakly competent lithology (as shown by steep erosional margins), but others may be patches of loose material. This thin surficial material has a maximum measured thickness of <5 m and, although predominantly below the spatial resolution (18 m/pixel) of CRISM, display no phyllosilicate spectral signatures. Dmd units drape underlying topography overlying boundaries and fractures in the clay-bearing units. However, these discrete patches do not appear on the Adru, where the surface roughness seemingly precludes its formation or observation. Regionally, the Dmd may represent the most geologically recent depositional events and its discontinuous nature might reflect both its friable nature and active, erosional processes (Quantin-Nataf et al., 2021; Mandon et al., 2021; Fawdon et al., 2023b).

Following on from the previous study targeting Oxia Planum (Favaro et al., 2021), this paper aims to test hypotheses for location, orientation, and age of PBRs at four sites across the wider circum-Chryse region. We specifically investigate: (i) whether there is a consistent orientation pattern of PBRs around the Chryse basin, as was observed in Oxia Planum, and to describe any regional variability seen. We aim to explore whether PBR orientations match expected present-day wind patterns, or are instead controlled by regional topography (e.g., might PBR orientations be concentric to Chryse basin?); (ii) whether the age of PBRs can be better constrained by exploring superposition relationships between PBRs and other surface features; and (iii) whether there is a spatial correlation between PBR locations and those regions where detections of clay minerals (specifically Fe/Mg-rich phyllosilicates) have been made from orbit (Carter et al., 2023; Fig. 1). We meet these aims by performing measurements and observations in four large study areas around the margins of the Chryse basin (Fig. 1a). Finally, we discuss what our results mean for hypotheses of PBR formation and retention and speculate on the work the ExoMars *Rosalind Franklin* could undertake to clarify these orbital observations.

2. Methods

2.1. Study approach overview

We used Context Camera (CTX; 6 m/pixel; Malin et al., 2007), HiRISE (up to 25 cm/pixel), and CaSSIS (4.5 m/pixel) images in a regional survey to identify, digitize, and extract the orientations and morphometrics of PBRs in four study areas in the circum-Chryse region.

We then compared the formational wind directions inferred from PBRs to modelled contemporary winds on Mars using Global Circulation Model (GCMs) near surface (1.5 m above surface) winds, generated from reanalysis of thermal and dust opacity data (Holmes et al., 2020). These provide our best estimates of present-day winds across the Chryse Basin region.

We attempted to determine age constraints on PBR formation based on superposition relationships as inferred from geomorphological observations made using HiRISE and CaSSIS images at Oxia Planum, where the highest fidelity data is available. This approach was necessary because the Circum-Chryse region has undergone multiple periods of deposition and erosion (McNeil et al. 2022; Quantin-Nataf et al., 2021), which makes crater-count dating of small erosional landforms almost impossible. Furthermore, across the region, PBRs crop out in relatively small areas (<1000 km^2; the minimum are required for acceptable crater counts; Warner et al., 2015), further complicating crater-based age determinations.

Finally, to investigate if there is a spatial correlation between PBR locations and regions of Fe/Mg-rich phyllosilicate-bearing terrain, we compared our survey of PBRs to the extent of OMEGA detections presented in Carter et al. (2023).

These approaches are explained in detail in the following sections.

2.2. PBR survey across the circum-Chryse region

Four study areas were selected as regions to conduct PBR surveys: Oxia Planum, Maja Valles, Hypanis Vallis, and Aram Chaos (Fig. 1). The sites were defined to be (i) in or around the Chryse Basin margin area, (ii) to contain a variety of topography and relief elements, (iii) to be large enough for variations in PBR orientation to be observed (should they be present) and (iv) to contain areas with and without OMEGA detections of Fe/Mg-rich phyllosilicate minerals to investigate whether the coincidence of PBRs in these terrains was unique to Oxia Planum. To achieve this, we used the global map of Fe/Mg-rich phyllosilicate minerals detected by OMEGA presented in Carter et al. (2023) and clipped its extent to cover the circum-Chryse region. The spatial resolution of OMEGA ranges from 300 m/px to 4 km/px but Carter et al. (2023) note that the higher resolution OMEGA detections were rarely used in the creation of the global database, as they constitute a minor contribution to surface coverage. Instead, datasets with kilometer scale resolution were used. OMEGA data have near-global coverage at 2 km/pixel, and therefore lend themselves well to regional studies and are appropriate data to use here.

Each study area was centered around the OMEGA detections in that region and divided into a grid system of 10×10 km squares. The grid was designed to assist the survey, allowing each study area to be searched systematically. Following the creation of the gridded study areas, the OMEGA detection data was removed from the GIS so as not to bias the PBR survey. Then, a manual search for PBRs based on linear ridge morphology (shape and size) and albedo in HiRISE and CTX images (after Favaro et al., 2021) was performed. Because we found PBRs to be a widespread, ubiquitous feature on the landscape, we did not digitize each PBR crestline; for each grid square, we manually selected between 3 and 200 PBR crestlines to digitize (digitizing the straight-line trace of the crestline ridge), with more examples digitized in grids that had more PBRs, and all PBRS where grid squares only contained a few examples. Where a grid square contained several discrete regions or 'fields' of PBRs (with some grid squares containing multiple fields of PBRs) we digitized

at least three representative PBRs from each field. This method of 'actively selected digitization' was preferred over a random or sub-grid sampling strategy because the PBRs are not themselves continuous across each study area, nor are they randomly distributed. Instead, they occur in small, discrete fields in some regions, but in larger accumulations in others. Therefore, we did not want to fail to sample each field. Digitizing was performed at a map scale of at least 1:2000 in HiRISE images and 1:10,000 in CTX images to acquire a representative sample.

Following the PBR survey, we re-introduced OMEGA detections into our GIS and classified the PBRs as being found on Fe/Mg-rich phyllosilicate-bearing terrain or being found on non-Fe/Mg-rich phyllosilicate-bearing terrain. To minimize the effects of OMEGA's low spatial resolution, obscuration by surface dust, and possible underestimation of the true extent of Fe/Mg-rich phyllosilicates, we buffered OMEGA detections by 5 km (Bibring et al., 2006; Murchie et al., 2007; Carter et al., 2023; for an example, see Fig. 2). Indeed, if the geomorphology of bedrock terrains that correlate with positive OMEGA Fe/Mg-rich phyllosilicate detections in Oxia Planum (e.g., Mandon et al. 2021) is indicative of the extent of Fe/Mg-rich phyllosilicates, then the extent of this terrain is probably more widespread in our study areas than is currently quantified; we present both non-buffered and buffered observations in Section 3.4.

2.3. Global Circulation Model Outputs – testing whether PBR orientation matches contemporary wind direction

Wind speeds, directions, stresses, and other meteorological conditions were generated using a Mars global circulation model (MGCM). The MGCM is based on the UK version of the Planetary Climate Model first described by Forget et al. (1999) and developed in a collaboration with the Laboratoire de Météorologie Dynamique, the Open University, the University of Oxford and the Instituto de Astrofisica de Andalucia. This model uses a largely shared set of physical parameterizations coupled to a spectral dynamical core (Hoskins and Simmons, 1975) and a semi-Lagrangian, conservative advection scheme (Newman et al., 2002). For the experiments described here a moderate 'climate simulation' resolution was used: in the vertical, 25 σ-levels ($\sigma = p/ps$, where p is the atmospheric pressure and ps the surface pressure) were distributed below about 80 km altitude, with the lowest level a few meters above the surface. In the horizontal, the MGCM was run with a triangular horizontal truncation at a total wavenumber 31, with nonlinear products calculated on a $3.75^\circ \times 3.75^\circ$ grid and two-hourly records of all model variables made on a $5^\circ \times 5^\circ$ grid.

The MGCM is otherwise the same as that used to generate the OpenMARS reanalysis database (Holmes et al., 2020), but no data assimilation was used for these experiments. Instead, the MGCM dust distribution was forced towards total column optical depths in an

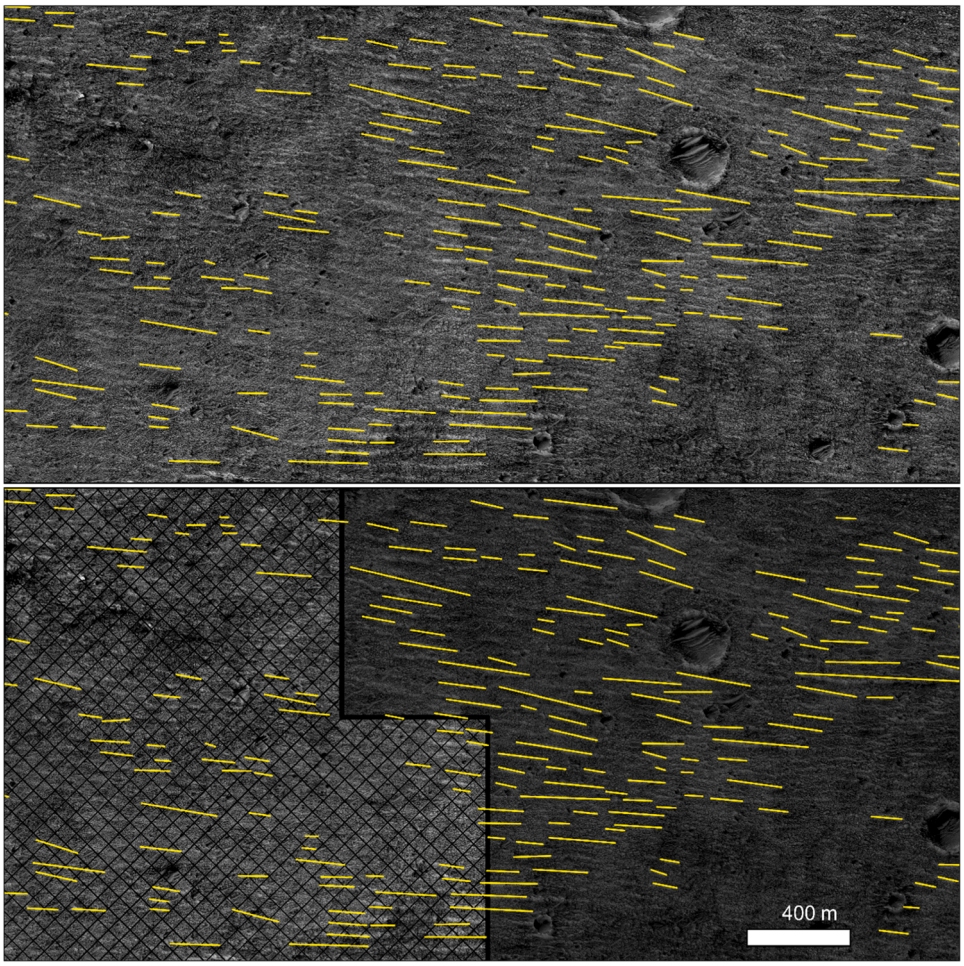

Fig. 2. An illustrative example behind the motivation for applying a buffer to the OMEGA detections. The upper panel shows a field of 209 PBRs, digitized here in yellow (ESP_044956_18 [left] and ESP_044956_1980 [right], centred at 24.44°W, 17.76° N in ESP_044956_1980). The lower panel shows the extent of OMEGA Fe/Mg-rich phyllosilicate mineral detections (in the shaded portion on the right) and the buffer (crosshatch) applied to these detections. PBRs in the cross-hatched area are part of the same population of PBRs that overlap with OMEGA detections, but would not be considered to occur on Fe/Mg-rich phyllosilicate-bearing terrain based on OMEGA detections alone. By applying a buffer to the OMGEA detections, all PBRs in the scene, which belong to the same population and are found on the same geologic surface, are counted as occurring on Fe/Mg-rich phyllosilicate-bearing terrain.

annually repeating cycle of a Mars Year 24-like dust distribution (Montabone et al., 2015), with the year numbering following Clancy et al. (2000). In Mars Year 24, there was a broadly typical annual dust cycle with a clear northern spring and summer and larger, regional storms in northern hemisphere autumn and winter, but no major planet-encircling dust event. The MGCM was run at five values of planetary obliquity, o = 5°, 15°, 25° (close to the present-day value of 25.2°), 35°, and 45°, but with other parameters (orbital eccentricity, 0.0935, and time of perihelion, at areocentric longitude = 251°) set at their present-day values, which is consistent with the annual dust cycle used.

The MGCM was run at these five obliquity configurations for 20 Mars years, with data being recorded during the 20th year only, having checked that the MGCM had a stable annual cycle ten years into each experiment. Meteorological variables were bi-linearly interpolated in the horizontal from the MGCM grid to each location used here, with the surface pressure adjusted hydrostatically using the air temperature profile at that location and time from the MGCM envelope orography to the local height of the surface above the reference aeroid, determined from the 1/32° MOLA topographic dataset (Smith et al., 2003). The wind profile was used to determine the windspeed at 1.5 m above the surface, the friction velocity and hence the surface stress (following eqn. 1, Hébrard et al., 2012) assuming a logarithmic wind profile in neutral conditions (Priestley, 1959; Read et al., 2017) and an aerodynamic roughness length of 0.01 m at each location. To examine wind direction, following Favaro et al. (2021), we use both the dominant wind direction

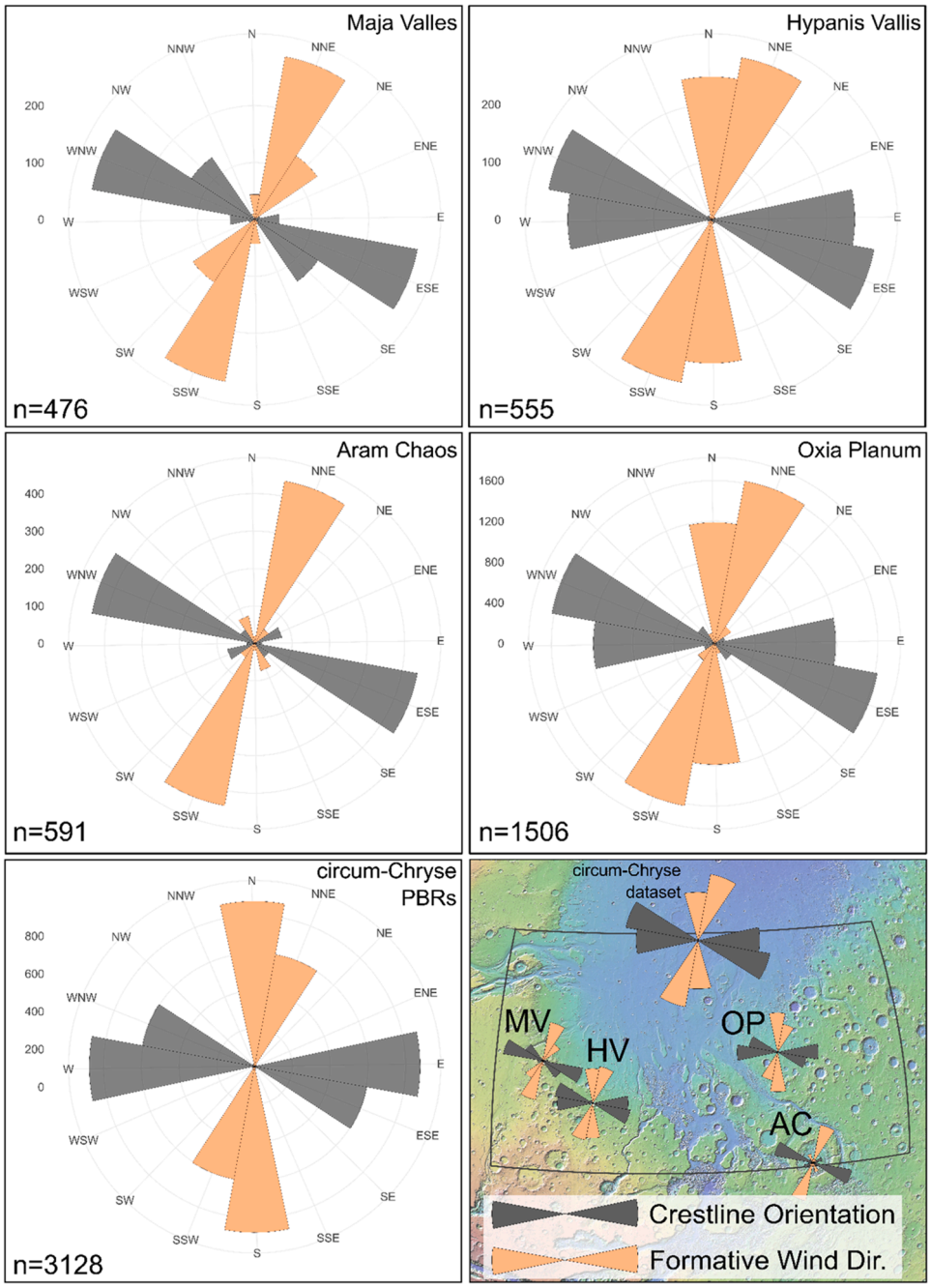

Fig. 3. PBR orientation (180° ambiguity; grey) and inferred formative wind direction (orange) roses of all digitized PBR crestlines at Maja Valles (MV), Hypanis Vallis (HV), Aram Chaos (AC), and Oxia Planum (OP) and as a composite across the region. Values on the concentric circles denote frequency of occurrence. Summary panel demonstrates a consistent pattern of crestline orientation across the circum-Chryse region.

from the model runs, and the dominant wind direction of the strongest 5 % of modelled winds. This allows us to compare PBR orientation with both the "typical" wind direction and those associated with the strongest winds most likely to lift particles in saltation and cause erosion.

3. Results

3.1. PBR orientation and length

Along-crestline orientations for 3128 PBRs were digitized and measured across the four study sites (Oxia Planum: 1506 PBRs; Maja Valles: 476 PBRs; Hypanis Vallis: 555 PBRs, Aram Chaos: 591 PBRs).

3.1.1. Orientation

Taking into account 180° of ambiguity, we found PBR crestlines at all four sites to have a dominant orientation of E-ESE/W-WNW (74 % of PBRs at Oxia Planum; 66 % of PBRs at Hypanis Vallis) or ESE-SE/WNW-NW (70 % at Maja Valles; 53 % at Aram Chaos; Fig. 3 Taken together, 85 % of PBR crestlines across the basin were oriented between E/W and ESE/WNW.

Because erosional PBRs develop perpendicular to dominant winds (Montgomery et al., 2012; Hugenholtz et al., 2015), we were also able to infer the wind directions which abraded the PBRs at each site. While there is some variability in the dominant wind direction, the large majority of PBRs across the basin would have developed from winds blowing from the S-SSW towards the N-NNE, or from the N-NNE towards the S-SSW.

3.1.2. Length metrics

PBR along-crestline lengths (Table 1) range from ~19 to ~916 m (both found in Oxia Planum). PBRs have an average length of 151 m across the study sites, with 99 % of all PBRs being shorter than 592 m. These results, especially in Maja Valles, Hypanis Vallis, and Aram Chaos, may be biased towards large PBRs, owing to the resolution of CTX images and a dearth of HiRISE images outside the Oxia Planum landing ellipses.

3.2. Climate model outputs

We compared GCM winds at 1.5 m above the surface for martian Year (MY) 24 under current (25°), low (5° and 15°), and high (35° and 45°) obliquity conditions at all four sites (Figs. 4 and 5). GCM predictions for each obliquity are typified by variable wind speed and direction. All values discussed are found in Table S1.

Under current obliquity, no modelled wind speed exceeded 17 ms^{-1}, with 99% of wind speeds falling below 14 m s^{-1}. Wind speeds in low and high obliquity conditions saw marginally stronger modelled winds, reaching ~25 m s^{-1} at Hypanis Vallis. Over the course of a Mars year, winds at each site exhibited substantial directional variability at each obliquity scenario (Figure 5 and S2), but with dominant trends emerging. Under current obliquities, winds blowing from between the SE and WSW were more often modelled than any other direction. In the case of Maja Vallis, winds blowing from the SW-WSW occurred in 26% of the records; at Aram Chaos, however, winds from the SSW-SW only accounted for 10% of the record. At 5° and 15° obliquities, winds most often originated from southwest and southeast, with an exception for Aram Chaos, whose dominant winds at 15° obliquity blow from the NNW-N. Dominant modelled winds at 35° and 45° obliquities were much more consistent, blowing from between the south and west-southwest. Additionally, PBR crestline orientation align most consistently with winds modelled for high obliquities, with a good agreement across the four study sites for dominant and 95th percentile winds modeled at 45° (Figure S1).

We also analyzed the wind directions associated with the 95th percentile of modelled wind speeds, as only the strongest winds are likely to entrain and transport aeolian materials and drive erosion. We found that these winds originated between the north-northwest and north-northeast more often than any other wind direction (16 out of 20 records).

Table 1
Summary of PBR along-crestline length (L) characteristics across all four study sites, and as a function of the entire record. n is the number of PBRs measured for each record.

	n	L_{min}	$L_{50\%}$ (m)	$L_{99\%}$ (m)	L_{max} (m)
Oxia Planum	1506	19	151	684	916
Maja Valles	476	35	131	403	513
Hypanis Vallis	555	56	159	563	903
Aram Chaos	591	57	163	514	712
Entire Record	3128	19	151	592	916

3.3. Observations relevant to PBR age

In addition to the regional survey of PBRs, observations constraining the age of PBRs were made using HiRISE and/or CaSSIS images. The aim was to investigate which surface types and morphological features are and are not superposed by PBRs. These observations are generally from the Oxia Planum *ERFR* landing site area, where the HiRISE coverage is greatest, but also include examples from the wider region. Fig. 5 highlights the lines of evidence collected to constrain the age of PBRs. Examples of PBRs seen superposing or set within fluvial sinuous ridges, that are themselves formed of the Oxia Planum clay-bearing materials (Davis et al., 2023), are shown in Fig. 5a. A tentative identification of PBRs forming concentrically to (and presumably after) a Noachian-aged mound (see McNeil et al., 2021; McNeil et al., 2022) is shown in Fig. 5b, while PBRs that appear to be being exhumed from beneath an eroded crater are shown in Fig. 5c. PBRs appear better defined in some clay-bearing materials than others that superpose them; Fig. 5d shows an example of such a relationship in which the bluer, overlying layer has many fewer PBRs in it than the underlying paler surface. Fig. 5e shows PBRs being superposed by a thin layer of dark material that is similar in appearance to Adru units. That the PBRs show extensive fractures but that the fractures are not exploited by wind erosion (Fig. 5f), suggest the PBRs formed before the fractures.

3.4. PBR spatial distribution compared to Fe/Mg-rich phyllosilicate-bearing terrains

The comparison between the distribution of Fe/Mg-rich phyllosilicate-bearing terrain and PBR distribution in each study area is presented in Table 2 and Fig. 7. Both the unbuffered and buffered calculations are presented.

4. Discussion

4.1. Wind regimes associated with PBR formation across the circum-Chryse region

PBRs demonstrate consistent crestline orientations across a 2.5 million square kilometer area of the circum-Chryse region (Fig. 1). Nearly 86 % of PBRs studied are oriented between E/W and ESE/WNW (180° ambiguity: Fig. 3). Following the usual assumption that PBRs form transverse to winds (Montgomery et al., 2012; Hugenholtz et al., 2015), they would therefore have been abraded by winds blowing between from the S/SSW towards the N/NNE or from the N/NNE towards the S/SSW. The consistent orientations of the PBRs suggest that they either formed due to time-integrated sediment transport vectors (i.e., long-term synoptic wind patterns), and/or that they formed on a surface with low relief, such that little local wind deflection occurred. We note that TARs can also show low variability in orientations across large areas (across nearly 1000 km in Meridiani Planum; Berman et al., 2011), so

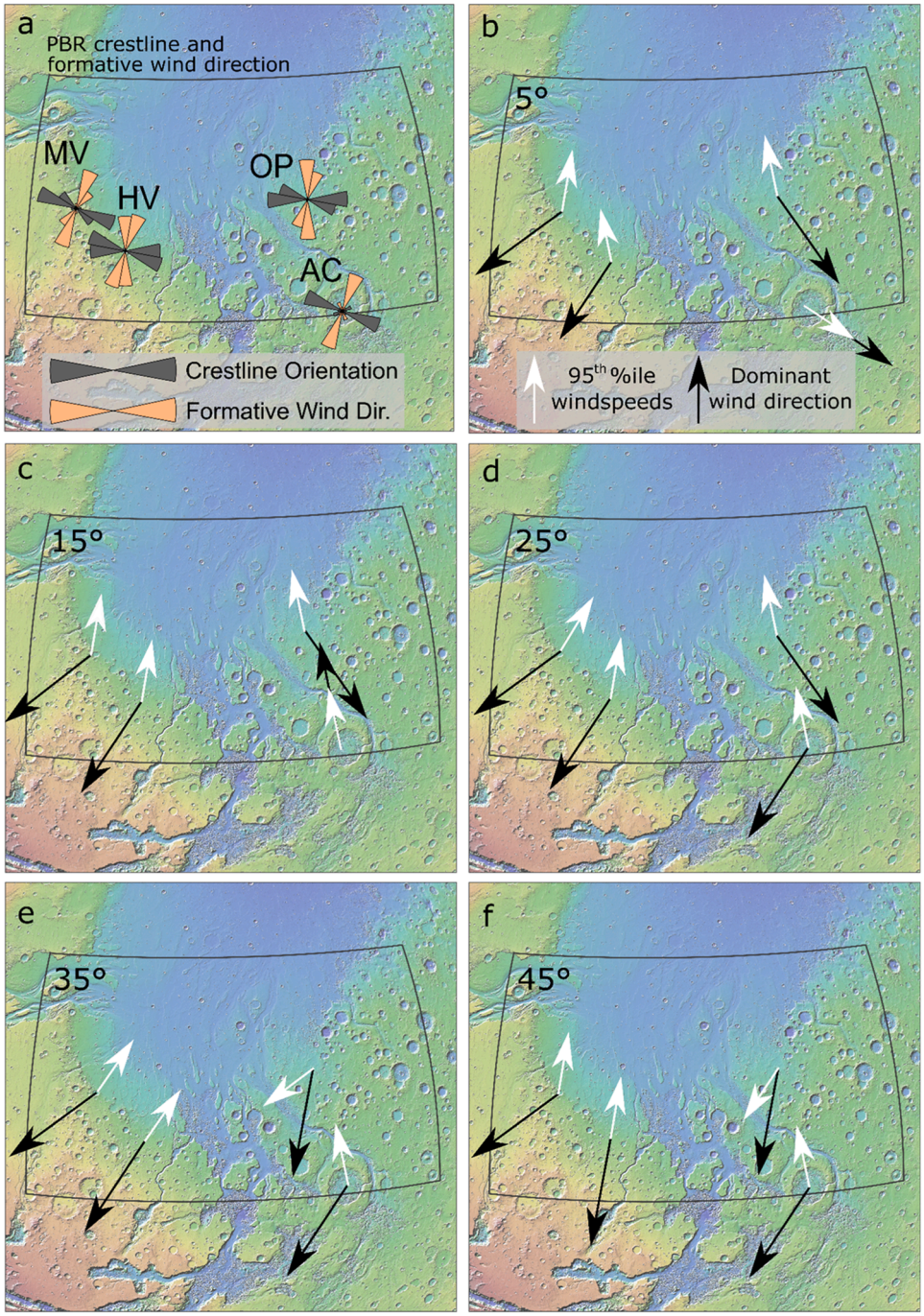

Fig. 4. Inferred and modelled wind directions at Maja Valles (MV), Hypanis Vallis (HV), Aram Chaos (AC), and Oxia Planum (OP) from (a) PBR orientations (Fig. 3) and (b-f) GCM outputs at varying obliquities. Black arrows show the dominant (mode; binned at 22.5° increments from 0° to 360°) wind direction from the whole GCM output at the centre of each study area. White arrows show the most frequently modelled the wind directions associated with only the 95th percentile windspeed outputs from the GCM.

this orientation pattern is consistent with PBR formation by the Hugenholtz model; Hugenholtz et al., 2015).

At Oxia Planum, Favaro et al. (2021) digitized the crestlines of 10, 753 TARs and found that winds blowing between the NW-NNW towards the SE-SSE were responsible for their formation (see Section 4.1.2 and Fig. 9 in Favaro et al. [2021]). TAR formative wind direction in Oxia Planum does not align with proposed PBR formative wind directions. Similarly, PBR orientations measured in this study do not match GCM outputs for present-day climate conditions but better match model winds from some higher obliquity GCM model runs. These high obliquity conditions have been rare or non-existent in the past few millions years, but were more frequent >5 million years ago (Laskar et al., 2004). Taking these results together, we infer that PBRs are not contemporary features and instead are directional indicators of a paleowind regime no longer effecting the region. Based on this evidence we can also speculate that the regional wind regime shift at Oxia Planum would have also affected the wider circum-Chryse region as the regional population of PBRs exhibit consistent orientations. Furthermore, given how consistent local-to-regional PBR orientations are, it seems likely that the PBRs around Chryse all formed around the same time under a regionally consistent wind regime. If they had formed at very different times, a wider range of PBR orientations would be expected, as shown by the

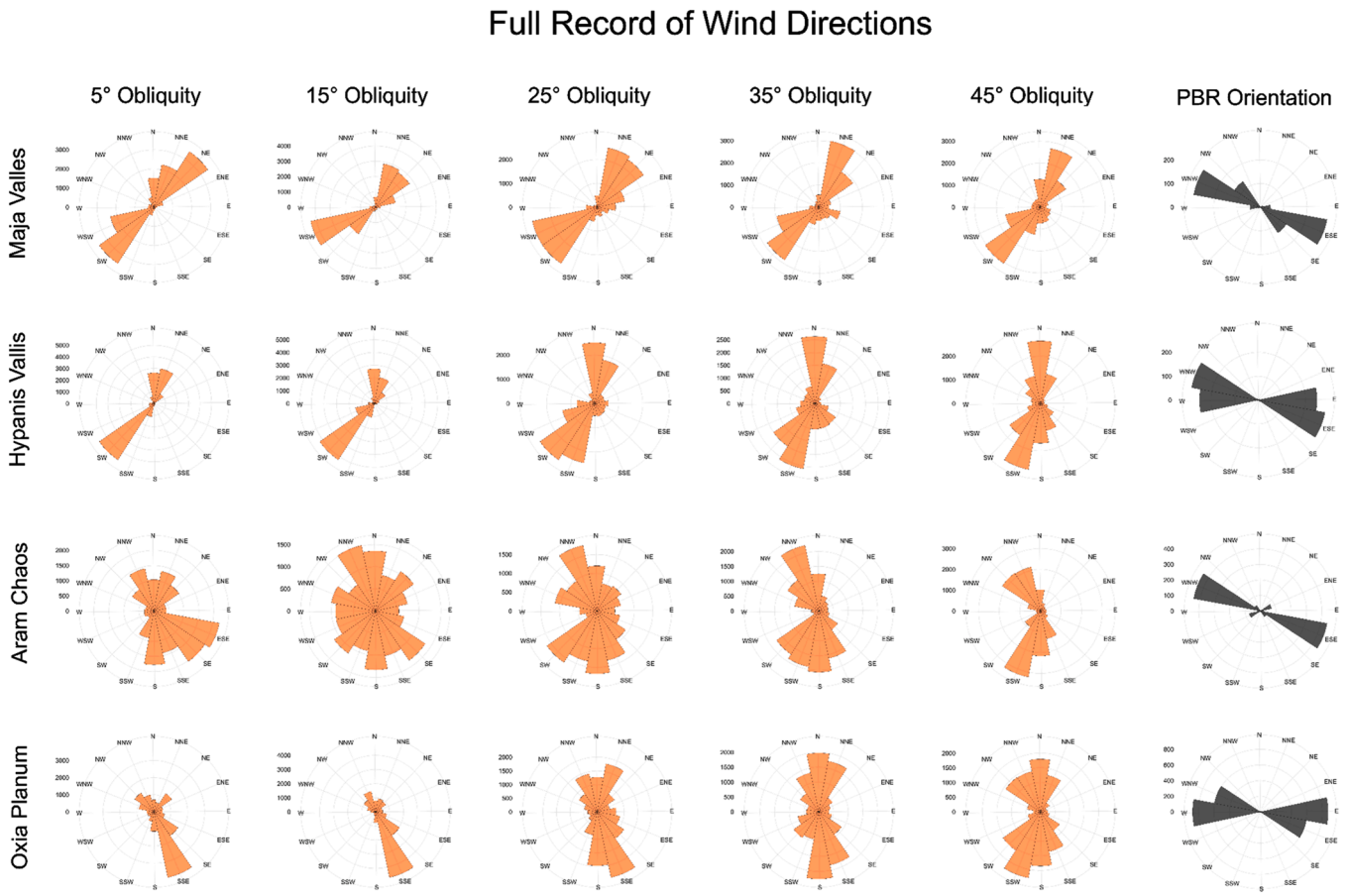

Fig. 5. Modelled wind direction roses (orange) for MY24 at varying obliquities for the four study sites across the circum-Chryse region. Values on the concentric circles denote frequency of occurrence. PBR orientations are presented in grey.

different dominant and peak wind GCM wind directions found for different obliquity conditions.

4.2. *Constraints on PBR age and timing of formation*

Although the consistent pattern of PBR orientations is best explained by them forming at the same time under a regionally consistent wind regime, it is not clear *when* in the geologic record they formed. Furthermore, any inference about formation age is complicated by the fact that their spatial distribution could be controlled by (i) surface properties (e.g., if PBRs formed relatively recently but only in areas with specific surface properties), by (ii) atmospheric conditions (e.g., if PBRs formed only during a specific past climate period), by (iii) subsequent burial/erosion (e.g., PBRs could have formed over long periods on an extensive paleosurface which has not yet been re-exposed in some regions, or which has had all PBRs removed by erosion), or by (iv) a combination of these processes.

Here we summarize superposition relationships as inferred from geomorphological observations at Oxia Planum that provide constraints on the timing of PBR formation:

1. PBRs are often found in the fractured, layered, clay-bearing bedrock that crops out across much of Oxia Planum. This is thought to be 4.0 Ga in age (Quantin-Nataf et al., 2021), providing a maximum age for the PBRs.
2. Noachian-aged fluvial sinuous ridges throughout the Oxia basin are found partially exhumed from within the clay-bearing terrain (Fawdon et al., 2022; Davis et al., 2023). PBRs are found eroded into this material adjacent to, and on top of, the fluvial sinuous ridges, and therefore have formed during or after the period of exhumation (Fig. 6a).
3. Examples of PBRs being deflected by nearby mounds (Fig. 6b; McNeil et al., 2021) southwest of the *ERFR* landing ellipse, suggest that PBR orientation can be affected by topography. Given these mounds are thought to have been eroded into their present-day shape during the early- to mid-Noachian (McNeil et al., 2021, McNeil et al., 2022), these PBRs would have formed during or after this period.
4. A 2 km diameter, heavily eroded impact crater in the south of the landing site appears to be younger than PBRs around it: PBR orientations are not influenced by the crater, as would be the case if this topographic obstacle was in place before the PBRs formed (Fig. 6c), and no PBRs are seen on the remaining smooth crater ejecta. Here, we infer that the PBRs have been exhumed from underneath the ejecta blanket. PBRs with approximate E-W orientation can be seen as close as 300 m from the degraded crater rim, and the distal ejecta has clearly been removed by erosion: in modern martian craters of this diameter, the ejecta blanket is 15-65 m thick at 300 m from the rim (Golombek et al., 2006), so would have formed a continuous surface here were it not for erosion. Similarly, the rim of this crater is highly degraded, and although it is up to 60 m high in places, in others it is almost absent. In fresh craters of similar size, the rims are continuous and 60-150 m high (Golombek et al., 2006). The PBRs here would have been completely buried by ejecta following the impact event but, since then, tens of meters of rim and ejecta have been lost by erosion. If we assume a burial depth of 35 m and an Amazonian erosion rate of 1-10 nm/yr (Golombek et al., 2006), this requires a time of 3.5-35 Ga for the ejecta to be removed and perhaps even longer for the rim materials. Thus, this crater likely formed

Table 2
Comparison of the coincidence of PBRs to be found on Fe/Mg phyllosilicate-bearing terrain, as detected by OMEGA.

Site	Site total area (km^2)	Area of phyllosilicate detections (km^2/ % coverage)	Percentage (%) of measured PBRs in that area that coincide with Fe/Mg Phyllosilicate-bearing terrain	Ratio of the % of measured PBRs in an area coinciding with Fe/Mg Phyllosilicate-bearing terrain and the total area of that terrain in the study area*	Area of phyllosilicate detections (5 km buffer; km^2/ % coverage)	Percentage (%) of measured PBRs in that area that coincide with Fe/Mg Phyllosilicate-bearing terrain buffer region	Ratio of the % of measured PBRs in an area coinciding with Fe/Mg Phyllosilicate-bearing terrain and the total area of that terrain in the buffered study area*
Oxia Planum	52898	7549 (14%)	62%	4.4	21463 (41%)	78%	1.9
Maja Valles	29042	765 (3%)	13%	4.3	3509 (12%)	30%	2.5
Hypanis Vallis	34494	3130 (9%)	28%	3.1	9069 (26%)	55%	2.1
Aram Chaos	17784	5464 (31%)	25%	0.8	10881 (61%)	63%	1.0

* We would expect the ratio between PBR occurrence and phyllosilicate-bearing terrain to be 1 if PBRs were found randomly throughout the study area. Where values are greater than 1, PBRs occur more frequently on phyllosilicate-bearing terrain.

before the Amazonian. Even if the ejecta here were more erodible than the fresh Meridiani impact craters described by Golombek et al. (2006), it is unlikely to have formed later into the Amazonian, given its state of degradation. This suggests these PBRs did not form geologically recently but instead formed in or before the early Amazonian.

5. In some areas of Oxia Planum, PBRs can be seen cross-cutting low scarps and shallow-pits within the Fe/Mg-rich phyllosilicate-bearing bedrock. Sometimes, these regions have tonal variations in CaSSIS images which indicate a consistent stratigraphy (Fig. 6d). We infer that the PBRs could have formed during the erosion that created the subtle relief seen now. This provides evidence that PBR development occurred after both styles of clay-bearing material formed; in other words, the clay-bearing terrains here contain one or more paleosurfaces.
6. PBRs are more often found eroded into or close to Fe/Mg-rich phyllosilicate-bearing terrain (with the exception of Aram Chaos; Table 2) than they are in areas without this mineral detection. For example, in Oxia Planum, PBRs are not found eroded into the Adru unit, nor are they found in the region's widespread Dmd mantling deposits. This suggests either (i) the Fe/Mg-rich phyllosilicate-bearing surface materials were susceptible to the abrasion that formed PBRs while the Adru and mantling surface materials were not (assuming PBRs formed after these units), or (ii) the Adru and mantling units were deposited later, on top of PBRs (possibly with periods of burial and erosion between the two. We favor the second interpretation, because observed PBR orientation is not affected by higher relief patches of Adru or mantling materials, and, in a few locations, patches of mantling material appear to drape across PBRs (Fig. 6e), and thus seem to have been deposited after them.
7. Throughout Oxia Planum, extensive fracture patterns are seen to run uninterrupted across PBRs (Fig. 6f), indicating the fracturing of the bedrock occurred after PBRs developed. If fractures had developed before PBRs, we would expect winds to have exploited these weakness zones and would therefore see linear ridges following fracture lines.

From evidence presented here, especially the superposition (and later removal) of impact crater ejecta and the Adru, we suggest PBRs were eroded into a Fe/Mg-rich phyllosilicate-bearing Noachian paleosurface sometime after the late Noachian (as evidenced by points 1 through 3, and 5) and in or before the early Amazonian (as evidenced by points 4 through 7). There is no strong evidence against PBRs having formed even earlier, if they were then buried and re-exposed.

4.3. Comparison of PBR distribution with Fe/Mg-rich phyllosilicate materials

If PBRs were distributed randomly, we might expect to find them located on Fe/Mg-rich phyllosilicate-bearing terrains at a similar percentage rate as the distribution of Fe/Mg-rich phyllosilicate-bearing terrains within that study area. For Oxia Planum, Maja Valles, and Hypanis Vallis, the actual rate of correspondence is ~ 2.5-4 times higher (Table 2). We can conclude that PBRS are more likely to form in Fe/Mg-rich phyllosilicate-bearing terrains than in other terrain types in these study areas. Furthermore, to account for the fact that the OMEGA data used here are probably under-representative of the true extent of the Fe/Mg-rich phyllosilicate-bearing terrains, we can use the 5-km buffer data to show that PBRs are even more likely to form on or *near to* Fe/Mg-rich phyllosilicate-bearing terrains detected in OMEGA data. Fig. 7 and Table 2 demonstrate this tendency for PBRs to be found on Fe/Mg-rich phyllosilicate-bearing terrains at Oxia Planum, Maja Valles, and Hypanis Vallis.

The case for there being a spatial association is less strong for Aram Chaos, and instead PBRs appear to be associated more with the 'caprock' unit (Catling and Moore, 2003; Glotch and Christensen, 2005) in the

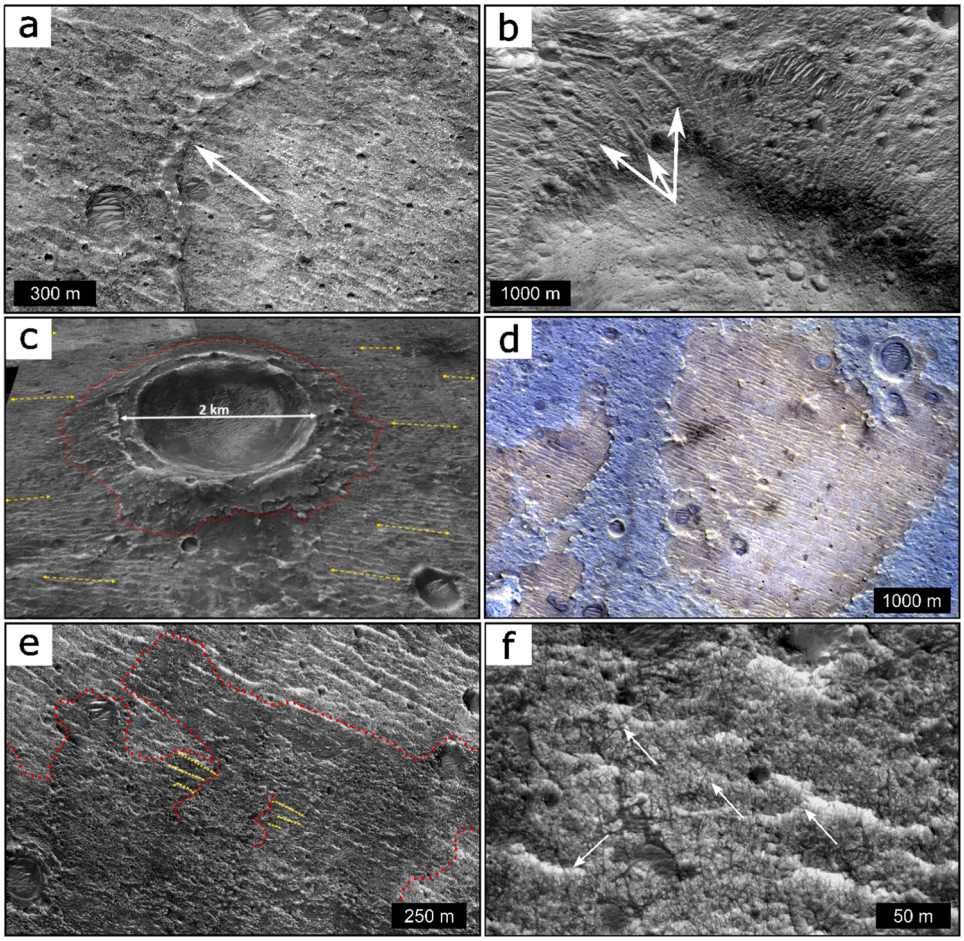

Fig. 6. Stratigraphic evidence for timing of PBR formation. (a) PBRs are seen to cross-cut fluvial sinuous ridges (denoted by white arrow; image centred at 24.2° W, 17.6° N in HiRISE image ESP_072017_1975). (b) PBRs are seen wrapping around a Noachian-aged mound (image centred at 25.3° W, 18.4° N in HiRISE image ESP_049703_1985). (c) HiRISE orthoimage mosaic draped onto a HiRISE 1 m DEM of a crater in southern Oxia Planum. North is up. Vertical exaggeration is 2 times. Yellow lines show trend of PBRs. Red line shows approximate contact between PBRs and degraded ejecta. (d) CaSSIS image exemplifying the absence of PBRs on non-Fe/Mg-rich phyllosilicate-bearing surfaces (purple) and their abundance on Fe/Mg-rich phyllosilicate-bearing surfaces (bright white/yellow). It also suggests PBRs formed at the same time, or after the erosion which eroded out the different layers within the Fe/Mg-rich phyllosilicate terrain (image centered at 25.8° W, 17.2° N in CaSSIS image MY36_016394_162_0). (e) HiRISE image showing dark, rough material draping the area (boundary denoted by red dashed outline) with three PBRs (yellow dashed lines) appearing on either side of an accumulation of the material. The inset figure provides context without annotations (main image centered at 24.27° W, 18.05° N in HiRISE image ESP_039299_1985). (f) Fractures (identified by white arrows) are seen crosscutting and running through PBRs (image centered at 24.28° W, 18.08° N in HiRISE image ESP_039299_1985).

west and southwest of the study area than with Fe/Mg-rich phyllosilicate-bearing terrains. In Mars Global Surveyor Thermal Emission Spectrometer (MGS-TES) data, this capping layer presents as >15% sheet silicate/glass, and therefore could contain phyllosilicates. However, this detection is not made by OMEGA. Dust covering Aram Chaos may explain the lack of detection here, as dust could obscure instrument absorption bands and mask hydrous clay signatures (Ody et al., 2012).

The observed correlation between PBRs and Fe/Mg-rich phyllosilicate-bearing terrains leads to the reasonable inference that the properties of these terrains is conducive to PBR formation.

This in turn suggests a similar mechanical property of the Fe/Mg-rich phyllosilicate-bearing terrains across the circum-Chryse region; one which experienced a common depositional and/or diagenetic or alteration history. This finding is not without precedent. The most conspicuous PBRs in Gale Crater have also found to be in the clay-bearing unit of Aeolis Mons (Mount Sharp; Milliken et al., 2014;Stack et al., 2022; Bennett et al., 2023).

We can provide a reasoned interpretation of the terrain's characteristics by drawing upon terrestrial field studies of PBRs in Northwestern Argentina. There, PBRs were found eroded out of low density, mechanically weak materials (ignimbrites), and genetically linked to megaripple cover which blankets the area. If PBRs at Oxia Planum, and throughout the circum-Chryse region, formed in a manner similar to PBRs in Argentina, it might be expected that any evidence of such a Hesperian/early Amazonian landform would have been eroded out of the rock record. However, because we still see PBRs on the surface of Mars today, and that they originally formed in a friable material, as on Earth, we can postulate that the Fe/Mg-rich phyllosilicate-bearing terrains throughout the region must have undergone cementation and alteration that left the material mechanically stronger than the surrounding terrain. Another, more speculative possibility is there was a progressive development of a lag of coarser, or more abrasion-resistant material at the surface that protected the PBR forming material. Either process would have resulted in the PBR-bearing terrain becoming more erosion resistant than the areas surrounding them, but we favor the early cementation theory, as this fits our observations of PBR-bearing surfaces being revealed in erosional windows.

We may also speculate that terrain at Oxia Planum where positive Fe/Mg-rich phyllosilicate detections have been made could be indicative of an ignimbrite. Based on terrestrial field studies and observations of PBRs in the circum-Chryse region, this proposed mechanism for the retention of PBRs is consilient with terrestrial field observations and

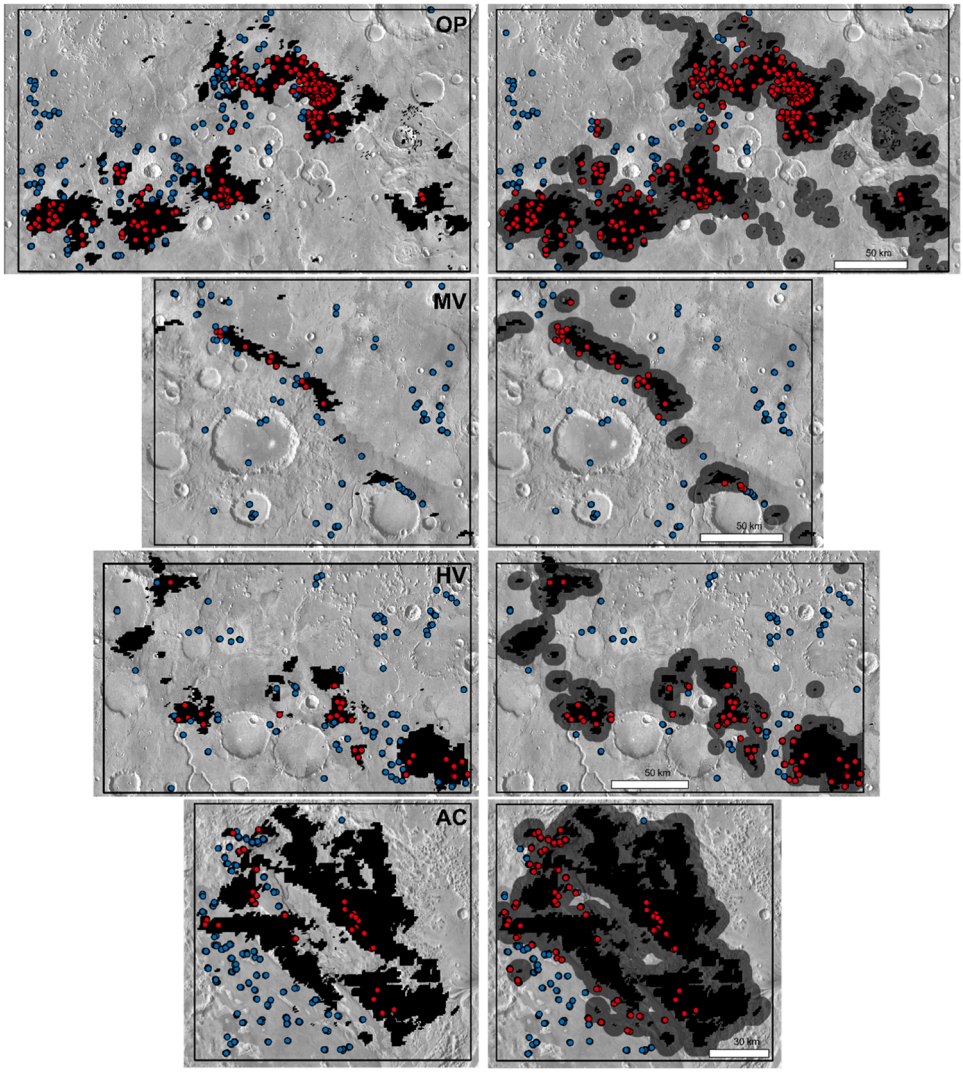

Fig. 7. PBR observations and OMEGA detections (left) and OMEGA detections with a 5 km buffer (right) of Fe/Mg-rich phyllosilicate-bearing terrain at Oxia Planum (OP), Maja Valles (MV), Hypanis Vallis (HV) and Aram Chaos (AC). Red markers denote PBRs intersecting Fe/Mg-rich phyllosilicate-bearing terrain; blue markers denote PBRs found outside these detections.

martian remote-sensing data and constitutes one mechanistic hypothesis for the Fe/Mg-rich phyllosilicate-bearing terrain which could be studied by the *Rosalind Franklin* rover. It is also important to note that, assuming the Hugenholtz et al (2015) model for PBR formation holds true, the vast fields of PBRs seen today around the margins of Chryse Planitia would have had to have been covered by similarly large seas of TARs for the PBRs to form. Although such huge TAR seas are not seen today on Mars, there seems to be no reason why this could not have been the case in the ancient past, especially given the relatively ancient formation age of PBRs and the length of time available for those TARs to be dispersed by wind. In fact, the occurrence of very large TAR fields in the ancient past is consistent with what we know about the Noachian environment. There would have ample supply of sand-grade material from the erosion of fluvial deposits (especially in Arabia Terra; cf. Craddock and Maxwell, 1993; Hynek et al., 2001; Evans et al., 2010; Davis et al., 2016, 2019). Also, as atmospheric density was probably higher during the Noachian, it is likely that surface wind shear stress and sediment flux potential would have been greater in the past too, allowing large fields of aeolian bedforms to accumulate and disperse on (geologically) short timescales as climate varied (e.g, Halevy and Head, 2014; Wordsworth, 2016; Kite et al., 2017). If very large TAR fields were present around Chryse Planitia in the distant past, then it is likely that the ultimate sink for their sediment was the northern plains, assuming sediment transport followed regional slope, or within the higher-relief cratered terrains to the south if not.

4.4. Implications for the ExoMars Rosalind Franklin rover mission

The identification of PBRs on Fe/Mg-rich phyllosilicate-bearing terrain across at least three out of four study sites examined suggests that the circum-Chryse region may have a shared common history of deposition, diagenesis, or alteration that resulted in similar mechanical properties. At Oxia Planum, this possibility can be investigated by *in situ* measurements and observations made by instruments aboard the *Rosalind Franklin* rover, including CLUPI (the Close-Up Imager Camera; Josset et al., 2017) and Ma_MISS (Mars Multispectral Imager for Subsurface Studies; De Sanctis et al., 2017).Considering the region does not have widespread geologic interpretations, this work is among the first attempts to draw regional correlations and could therefore have basin-wide implications.

In situ observations of PBRs by the PanCam camera (Coates et al., 2017) may help clarify the formative wind direction which would have been necessary to form the feature. PanCam would also be able to image the surrounding terrain and characterize the aeolian environment

(presence/absence of granular material, the nature of a PBR capping layer, an evaluation of unconsolidated or modern bedforms), which would in turn offer insight into the nature of PBRs in the area.

If winds at Oxia Planum are strong enough to sustain even intermittent granular transport, PBRs would be active (although probably evolving very slowly) aeolian landforms and could retain signals of contemporary wind directions in the form of the presence or absence of varnish, and abrasion textures on their flanks. For example, in northwestern Argentina, the stoss (upwind and actively abrading) side of PBRs are devoid of the thin varnish which has coated the lee (downwind) slope (Hugenholtz et al., 2015). This difference in colour is clear *in situ*, but not always discernable or well defined in satellite images (Fig. 8). From orbit, it is unclear if PBRs at Oxia Planum have this stoss/lee characteristic, but oblique PanCam images would be able to capture the presence of a coating (through differences in colour), should it be present. PBRs in Argentina also retain abrasion texture indicative of a dominant wind direction, including grooves and aeolian rat-tails (Fig. 8b;Favaro et al., 2017). Abrasion textures captured by PanCam would provide compelling evidence for contemporary wind directions, which could then be used as inputs for local and regional wind models.

The utility of using in situ observations to support orbital data in elucidating PBR mechanics and origins is demonstrated by Curiosity rover's investigation into PBRs in Gale Crater. Stack et al. (2022) studied PBRs eroded into Fe-smectite-bearing terrain in the Glen Torridon region of Mount Sharp. Using HiRISE images and digital elevation models, they mapped PBRs in a GIS, and used Curiosity rover images to characterize PBR morphometrics and the geology they were observed in, compared PBRs to modern aeolian features, and evaluated "stratigraphic relationships between ridges [PBRs] and outcrops". Rover mobility data also contributed to their investigation of PBRs as Curiosity traversed "over ridge crests or up ridge flanks". Through in situ and orbital observations and analyses, Stack et al. (2022) concluded that the PBRs in Glen Torridon were not contemporary features (based on morphometry, lithification of the ridges, an armouring layer comprised of pebbles and cobbles unlikely to have been mobilized by modern-day winds, and minor rover wheel sinkage compared to unconsolidated TARs and megaripples elsewhere on the traverse), nor ancient lithified bedforms (as regional bedrock units in the area are incorporated within PBRs, and their orientation does not align with the orientation of bedding where it is exposed and observable). Rather, they suggest the Glen Torridon PBRs developed during the erosion of Mount Sharp and a 'significant' amount of time following the emplacement of the bedrock units observed there today. Although Stack et al. (2022) did not ascribe an age to these PBRs, Bennett et al. (2023) suggests smectites could have formed during the Hesperian, thereby suggesting the PBRs in the Glen Torridon could have formed in the Hesperian when wind drove geomorphic alterations to the landscape, or at some point during the Amazonian. A similar investigation of PBRs at Oxia Planum with the Rosalind Franklin rover's suite of cameras and instruments could also collate these lines of evidence to better constrain the development of PBRs in the region, the geologic origin of the material they are found in (e.g., is the material an ignimbrite that was cemented following formation?), and their age in the geologic record.

5. Conclusions

This work investigates the orientation and distribution of PBRs at the Oxia Planum ExoMars *Rosalind Franklin* rover landing site and across the wider circum-Chryse region, as well as their propensity to be found on Fe/Mg-rich phyllosilicate-bearing terrains. Based on our mapping and

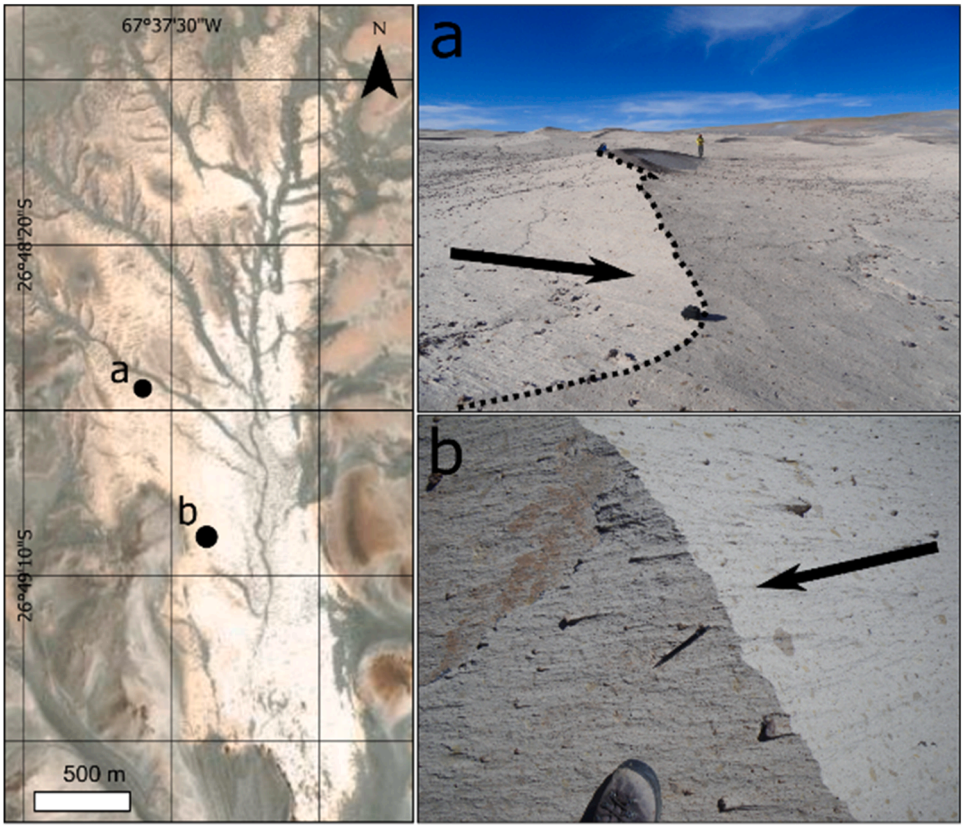

Fig. 8. PBRs in the Abra Poméz region of Northwestern Argentina. Varnish on PBRs, as seen in (a), is not always visible from orbit, yet clearly denotes dominant wind direction from in situ observations. A megaripple pulling away from the crest is visible in the background. (b) Microabrasion features like ARTs indicate abrasion on both sides of the PBR crest. In this example, the lack of varnish on the windward side connotes the active surface. Arrows denote dominant wind direction. (Photos credit: T. Barchyn).

examination of PBRs in HiRISE, CTX, and CaSSIS images and comparison with OMEGA detections of hydrous mineralogy (Carter et al., 2023), we present the following 5 conclusions:

1. PBRs across the circum-Chryse region display consistent directionality, with the majority (85%) of crestlines oriented between E/W and ESE/WNW (180° ambiguity). This suggests regional unimodal winds blowing from the S-SSW towards the N-NNE, or from the N-NNE towards the S-SSW (180° ambiguity) were responsible for PBR abrasion. This also suggests the PBRs around Chryse Basin formed at the same time, as it seems unlikely that PBRs forming far apart in time would have such consistently similar orientations.
2. Modelled present-day wind directions for each of the four study sites do not agree with landscape-derived dominant wind directions as inferred from our measurements of PBR orientation. This suggests PBRs formed under regional wind conditions not expected for present-day Mars. To investigate whether PBR orientations better match atmospheric conditions likely to have occurred in the past, we compared PBR orientation to modelled winds from GCM runs performed with different obliquities. We find that PBRs orientations have a better match to winds modelled for higher ($\geq$ 35° to 45°) obliquities conditions than winds seen under today's obliquity (~25°). When only considering the strongest winds (>95th percentile), PBR orientations have a better match with winds modelled for times when obliquities were low (5-15°). Either way, these results suggest PBRs were not formed mainly by present day wind conditions.
3. Based on landscape-level and superposition observations of PBRs and the surrounding terrain, including fluvial sinuous ridges, mounds, craters, fractures, and their abundance in Fe/Mg-rich phyllosilicate-bearing terrains, we suggest PBRs were eroded into a paleosurface at a time after the late Noachian and in or before the early Amazonian.
4. The extreme consistency of PBR orientations suggests that they formed on a surface of low-relief, and/or due to time-integrated sediment transport vectors. This would be consistent with PBRs forming in the manner described by Hugenholtz et al. (2015). Also, arguably more speculatively, this observation is consistent with the PBRS having formed in a huge ignimbrite deposit, covered by a regional palaeo-TAR field.
5. Analysis of buffered and unbuffered OMEGA detections at Oxia Planum, Maja Valles, and Hypanis Vallis show PBRs are consistently found within Fe/Mg-rich phyllosilicate-bearing terrain.
6. The widespread nature of the coincidence of PBRs on Fe/Mg-rich phyllosilicate-bearing terrain is indicative of the emplacement of a regional clay-bearing unit with a consistent depositional, diagenetic, and/or alteration history across the circum-Chryse region that has led to a regionally extensive material with consistent lithology. Hypotheses tested at Oxia Planum with the rover's suite of instrumentation could therefore have regionally substantive implications about the nature of this material (e.g., if it is an altered ignimbrite deposit), and about when and how these rocks were exposed to the surface environment.

Data availability statement

GIS data products used to analyze PBRs are available for download online (10.21954/ou.rd.23586165). The standard data products used here are available from the NASA PDS (https://pds.jpl.nasa.gov/) and the ESA PSA (https://www.cosmos.esa.int/web/psa/psa-introduction). Calibrated CaSSIS can be found at 10.5270/esa-da0ic0t.

CRediT authorship contribution statement

Elena A. Favaro: Writing – review & editing, Writing – original draft, Visualization, Validation, Software, Project administration, Methodology, Investigation, Formal analysis, Data curation, Conceptualization. **Matthew R. Balme:** Writing – review & editing, Supervision, Resources, Project administration, Methodology, Funding acquisition, Formal analysis, Data curation, Conceptualization. **Joseph D. McNeil:** Writing – review & editing, Methodology, Formal analysis, Data curation. **Peter Fawdon:** Writing – review & editing, Visualization, Resources, Methodology, Data curation. **Joel M. Davis:** Writing – review & editing, Conceptualization. **Peter M. Grindrod:** Writing – review & editing, Formal analysis, Data curation. **Stephen R. Lewis:** Writing – review & editing, Software, Resources, Methodology, Formal analysis, Data curation.

Declaration of Competing Interest

The authors declare that they have no known competing financial interests or personal relationships that could have appeared to influence the work reported in this paper.

Acknowledgments

We thank Mackenzie Day, one anonymous reviewer, and especially Kathryn Stack Morgan for their throughful, thorough reviews of this research. EAF and MRB gratefully acknowledge UK Space Agency (UK SA) funding (ST/T002913/1, ST/ V001965/1 and ST/R001413/1). JMD acknowledges UK SA funding (ST/ R002355/1). PMG acknowledges UK SA funding (ST/R002355/1, ST/V002678/1, ST/L006456/1). PF acknowledges UK SA funding (ST/V001965/1 and ST/ R001413/1). SRL acknowledges UK SA funding (ST/T002913/1, ST/ R001405/1 and ST/ S00145X/1). CaSSIS is a project of the University of Bern funded through the Swiss Space Office via ESA's PRODEX program. The instrument hardware development was also supported by the Italian Space Agency (ASI) (ASI-INAF agreement no. I/018/12/0), INAF/Astronomical Observatory of Padova, and the Space Research Center (CBK) in Warsaw.

Supplementary materials

Supplementary material associated with this article can be found, in the online version, at doi:10.1016/j.epsl.2023.118522.

References

Bennett, K.A., Fox, V.K., Bryk, A., Dietrich, W., Fedo, C., Edgar, L., et al., 2023. The curiosity Rover's exploration of Glen Torridon, Gale Crater, Mars: an overview of the campaign and scientific results. Journal of Geophysical Research: Planets 128 (1), 1–31. https://doi.org/10.1029/2022JE007185.

Berman, D.C., Balme, M.R., Rafkin, S.C., Zimbelman, J.R., 2011. Transverse aeolian ridges (TARs) on Mars II: distributions, orientations, and ages. Icarus 213 (1), 116–130.

Bibring, J.P., Soufflot, A., Berthé, M., Langevin, Y., Gondet, B., Drossart, P., Forget, F., 2004. OMEGA: Observatoire pour la Minéralogie, l'Eau, les Glaces et l'Activité. In: Wilson, Andrew (Ed.), Mars Express: the scientific payload, 1240. ESA Publications Division, Noordwijk, Netherlands, pp. 37–49 scientific coordination: Agustin Chicarro. ESA SP-1240.

Bibring, J.P., Langevin, Y., Mustard, J.F., Poulet, F., Arvidson, R., Gendrin, A., et al., 2006. Global mineralogical and aqueous Mars history derived from OMEGA/Mars Express data. Science 312 (5772), 400–404. https://doi.org/10.2307/3845879.

Bowen, A.P., Bridges, J., Tornabene, L., Mandon, L., Quantin-Nataf, C., Patel, M.R., Pajola, M., 2022. A CaSSIS and HiRISE map of the Clay-bearing Unit at the ExoMars 2022 landing site in Oxia Planum. Planetary and space science 214, 105429.

Brossier, J., Altieri, F., De Sanctis, M.C., Frigeri, A., Ferrari, M., De Angelis, S., Costa, N., 2022. Constraining the spectral behavior of the clay-bearing outcrops in Oxia Planum, the landing site for ExoMars "Rosalind Franklin" rover. Icarus 386, 115114.

Carter, J., Loizeau, D., Quantin, C., Balme, M., Poulet, F., Gupta, S., et al., 2015. Mineralogic context of the circum-Chryse Planitia candidate landing sites for the ExoMars rover mission. In: Proceedings of the 46th Lunar and Planetary Science Conference.

Carter, J., Quantin, C., Thollot, P., Ody, A., Lozach, L. (2016). Oxia Planum: a clay-laden landing site proposed for the ExoMars rover mission: aqueous mineralogy and alteration scenarios. In: Proceedings of the 47th Lunar and Planetary Science Conference.

Carter, J., Riu, L., Poulet, F., Bibring, J. P., Langevin, Y., & Gondet, B. (2023). A Mars orbital catalog of aqueous alteration signatures (MOCAAS). Icarus, 389, 115164.

Catling, D. C., & Moore, J. M. (2003). The nature of coarse-grained crystalline hematite and its implications for the early environment of Mars. *Icarus*, 165(2), 277–300.
Clancy, R.T., Sandor, B.J., Wolff, M.J., Christensen, P.R., Smith, M.D., Pearl, J.C., et al., 2000. An intercomparison of ground-based mil-limeter, MGS TES, and Viking atmospheric temperature measurements: Seasonal and interannual variability of temperatures and dust loading in the global Mars atmosphere. J. Geophys. Res. 105, 9553–9571. https://doi.org/10.1029/1999JE001089.
Coates, A.J., Jaumann, R., Griffiths, A.D., Leff, C.E., Schmitz, N., Josset, J.L., Osinski, G. R., 2017. The PanCam instrument for the ExoMars rover. Astrobiology 17 (6–7), 511–541.
Craddock, R.A., Maxwell, T.A., 1993. Geomorphic evolution of the Martian highlands through ancient fluvial processes. J. Geophys. Res. Planets 98 (E2), 3453–3468.
Davis, J.M., Balme, M., Grindrod, P.M., Williams, R.M.E., Gupta, S., 2016. Extensive Noachian fluvial systems in Arabia Terra: implications for early Martian climate. Geology 44 (10), 847–850.
Davis, J.M., Gupta, S., Balme, M., Grindrod, P.M., Fawdon, P., Dickeson, Z.I., Williams, R.M., 2019. A diverse array of fluvial depositional systems in Arabia Terra: evidence for mid-Noachian to early Hesperian Rivers on Mars. J. Geophys. Res. Planets 124 (7), 1913–1934.
Davis, J.M., Balme, M.R., Fawdon, P., Grindrod, P.M., Favaro, E.A., Banham, S.G., Thomas, N., 2023. Ancient alluvial plains at Oxia Planum, Mars. Earth Planet. Sci. Lett. 601, 117904.
De Sanctis, M.C., Altieri, F., Ammannito, E., Biondi, D., De Angelis, S., Meini, M., et al., 2017. Ma-MISS on ExoMars: mineralogical characterization of the Martian subsurface. Astrobiology 17 (6–7), 612–620. https://doi.org/10.1089/ast.2016.1541.
Evans, A.J., Andrews-Hanna, J.C., Zuber, M.T., 2010. Geophysical limitations on the erosion history within Arabia Terra. J. Geophys. Res. Planets 115 (E5).
Favaro, E.A., Hugenholtz, C.H., Barchyn, T.E., 2017. Evolution and diagnostic utility of aeolian rat-tails: A new type of abrasion feature on Earth and Mars. Aeolian Research 28, 91–98.
Favaro, E.A., Balme, M.R., Davis, J.M., Grindrod, P.M., Fawdon, P., Barrett, A.M., Lewis, S.R., 2021. The Aeolian environment of the landing site for the ExoMars Rosalind Franklin Rover in Oxia Planum. Mars. J. Geophys. Res. Planets 126 (4). https://doi.org/10.1029/2020JE006723.
Fawdon, P., Grindrod, P., Orgel, C., Sefton-Nash, E., Adeli, S., Balme, M., Volat, M., 2021. The geography of Oxia Planum. J. Maps 17 (2), 621–637.
Fawdon, P., Balme, M.R., Davis, J.M., Bridges, J.C., Gupta, S., Quantin-Nataf, C., 2022. Rivers and lakes in Western Arabia Terra: the fluvial catchment of the ExoMars 2022 rover landing site. Earth Space Sci. Open Arch. (3) https://doi.org/10.1002/essoar.10507896.1.
Fawdon, P., Orgel, C., Sefton-Nash, E., Adeli, S., Balme, M., Davis, J., Vago, J., 2023a. The HiRISE scale map of the proposed landing site for the ExoMars Rosalind Franklin Rover in Oxia Planum. In: Proceedings of the 54th Annual Lunar and Planetary Science Conference, p. 2037, 2806.
Fawdon, P., Orgel, C., Adeli, S., Balme, M.R., Carter, J., Cremonese, G., Davis, J., Favaro, E., Vago, J.L., 2023b. Hypotheses and implications for the geological history of Oxia Planum. In: Proceedings of the 54th Annual Lunar and Planetary Science Conference, p. 2061, 2806.
Forget, F., Hourdin, F., Fournier, R., Hourdin, C., Talagrand, O., Collins, M., et al., 1999. Improved general circulation models of the Martian atmosphere from the surface to above 80 km. J. Geophys. Res. 104 (E10), 24155–24175.
Glotch, T.D., Christensen, P.R., 2005. Geologic and mineralogic mapping of Aram Chaos: evidence for a water-rich history. J. Geophys. Res. Planets 110 (E9).
Golombek, M.P., Grant, J.A., Crumpler, L.S., Greeley, R., Arvidson, R.E., Bell, J.F., et al., 2006. Erosion rates at the Mars Exploration Rover landing sites and long-term climate change on Mars. J. Geophys. Res. Planets 111 (12), 1–14. https://doi.org/10.1029/2006JE002754.
Halevy, I., Head III, J.W., 2014. Episodic warming of early Mars by punctuated volcanism. Nat. Geosci. 7 (12), 865–868.
Holmes, J.A., Lewis, S.R., Patel, M.R., 2020. OpenMARS: a global record of Martian weather from 1999 2015. Planet. Space Sci. 188 (May), 104962 https://doi.org/10.1016/j.pss.2020.104962.
Hoskins, B.J., Simmons, A.J., 1975. A multi-layer spectral model and the semi-implicit method. Q. J. R. Meteorol. 101 (429), 637–655.
Hugenholtz, C.H., Barchyn, T.E., Favaro, E.A., 2015. Formation of periodic bedrock ridges on Earth. Aeolian Res. 18, 135–144. https://doi.org/10.1016/j.aeolia.2015.07.002.
Hynek, B.M., Phillips, R.J., 2001. Evidence for extensive denudation of the Martian highlands. Geology 29 (5), 407–410.
Josset, J.L., Westall, F., Hofmann, B.A., Spray, J., Cockell, C., Kempe, S., et al., 2017. The close-up imager onboard the ESA ExoMars Rover: objectives, description, operations, and science validation activities. Astrobiology 17 (6–7), 595–611. https://doi.org/10.1089/ast.2016.1546.
Kite, E.S., Gao, P., Goldblatt, C., Mischna, M.A., Mayer, D.P., Yung, Y.L., 2017. Methane bursts as a trigger for intermittent lake-forming climates on post-Noachian Mars. Nat. Geosci. 10 (10), 737–740.
Laskar, J., Correia, A.C., Gastineau, M., Joutel, F., Levrard, B., Robutel, P., 2004. Long term evolution and chaotic diffusion of the insolation quantities of Mars. Icarus 170 (2), 343–364.
Loizeau, D., Mangold, N., Poulet, F., Bibring, J.P., Gendrin, A., Ansan, V., Neukum, G., 2007. Phyllosilicates in the Mawrth Vallis region of Mars. J. Geophys. Res. Planets 112 (E8).
Malin, M.C., Bell, J.F., Cantor, B.A., Caplinger, M.A., Calvin, W.M., Clancy, R.T., et al., 2007. Context camera investigation on board the Mars reconnaissance orbiter. J. Geophys. Res. E Planets 112 (5), 1–25. https://doi.org/10.1029/2006JE002808.
Mandon, L., Parkes Bowen, A., Quantin-Nataf, C., Bridges, J.C., Carter, J., Pan, L., et al., 2021. Morphological and spectral diversity of the clay-bearing unit at the ExoMars landing site Oxia Planum. Astrobiology 21 (4), 464–480. https://doi.org/10.1089/ast.2020.2292.
McEwen, A. S., Eliason, E. M., Bergstrom, J. W., Bridges, N. T., Hansen, C. J., Delamere, W. A., & Weitz, C. M. (2007). Mars reconnaissance orbiter's high resolution imaging science experiment (HiRISE). *J. Geophys. Res.*, 112(E5).
McNeil, J.D., Fawdon, P., Balme, M.R., Coe, A.L., 2021. Morphology, morphometry and distribution of isolated landforms in southern Chryse Planitia, Mars. J. Geophys. Res. Planets 126 (5), e2020JE006775.
McNeil, J.D., Fawdon, P., Balme, M.R., Coe, A.L., Thomas, N., 2022. Mounds in Oxia Planum: the burial and exhumation of the ExoMars Rover landing site. J. Geophys. Res. Planets 127 (11), e2022JE007246.
Milliken, R.E., Ewing, R.C., Fischer, W.W., Hurowitz, J., 2014. Wind-blown sandstones cemented by sulfate and clay minerals in Gale Crater, Mars. Geophys. Res. Lett. 41 (4), 1149–1154. https://doi.org/10.1002/2013GL059097.
Montabone, L., Forget, F., Millour, E., Wilson, R.J., Lewis, S.R., Cantor, B., Wolff, M.J., 2015. Eight-year climatology of dust optical depth on Mars. Icarus 251, 65–95.
Montgomery, D.R., Bandfield, J.L., Becker, S.K., 2012. Periodic bedrock ridges on Mars. J. Geophys. Res. Planets 117 (E3), E03005. https://doi.org/10.1029/2011JE003970.
Murchie, S., Arvidson, R., Bedini, P., Beisser, K., Bibring, J.P., Bishop, J., et al., 2007. Compact connaissance imaging spectrometer for Mars (CRISM) on Mars reconnaissance orbiter (MRO). J. Geophys. Res. E Planets 112 (5), 1–57. https://doi.org/10.1029/2006JE002682.
Newman, C.E., Lewis, S.R., Read, P.L., Forget, F., 2002. Modeling the Martian dust cycle, 1. Representations of dust transport processes. J. Geophys. Res. 107, 6.
Ody, A., Poulet, F., Langevin, Y., Bibring, J.P., Bellucci, G., Altieri, F., Manaud, N.C.E.J., 2012. Global maps of anhydrous minerals at the surface of Mars from OMEGA/MEx. J. Geophys. Res. Planets 117 (E11).
Quantin-Nataf, C., Carter, J., Mandon, L., Thollot, P., Balme, M., Volat, M., et al., 2021. Oxia Planum: the landing site for the ExoMars "rosalind Franklin" Rover Mission: geological context and prelanding interpretation. Astrobiology 21 (3), 345–366. https://doi.org/10.1089/ast.2019.2191.
Silvestro, S., Pacifici, A., Salese, F., Vaz, D.A., Neesemann, A., Tirsch, D., et al., 2021. Periodic bedrock ridges at the ExoMars 2022 landing site: evidence for a changing wind regime. Geophys. Res. Lett. 48 (4), 1–10. https://doi.org/10.1029/2020GL091651.
Stack, K.M., Dietrich, W.E., Lamb, M.P., Sullivan, R.J., Christian, J.R., Newman, C.E., et al., 2022. Orbital and *in-situ* investigation of periodic bedrock ridges in Glen Torridon, Gale Crater, Mars. J. Geophys. Res. Planets 127 (6), 1–33. https://doi.org/10.1029/2021JE007096.
Tanaka, K.L., Skinner, J.A., Dohm, J.M., Irwin, R.P., Kolb, E.J., Fortezzo, C.M., et al., 2014. Geologic Map of Mars, 3292. U.S. Geological Survey Geologic Investigations. Retrieved from. http://pubs.usgs.gov/sim/3292/.
Thomas, N., Cremonese, G., Ziethe, R., Gerber, M., Brändli, M., Bruno, G., et al., 2017. The colour and stereo surface imaging system (CaSSIS) for the ExoMars trace gas orbiter. Space Sci. Rev. 212 (3–4), 1897–1944. https://doi.org/10.1007/s11214-017-0421-1.
Volat, M., Quantin-Nataf, C., Dehecq, A., 2022. Digital elevation model workflow improvements for the MarsSI platform and resulting orthorectified mosaic of Oxia Planum, the landing site of the ExoMars 2022 rover. Planet. Space Sci. 222, 105552.
Warner, N.H., Gupta, S., Calef, F., Grindrod, P., Boll, N., Goddard, K., 2015. Minimum effective area for high resolution crater counting of martian terrains. Icarus 245, 198–240.
Wordsworth, R.D., 2016. The climate of early Mars. Annu. Rev. Earth Planet. Sci. 44, 381–408.
Yizhaq, H., Katra, I., Kok, J.F., Isenberg, O., 2012. Transverse instability of megaripples. Geology 40 (5), 459–462. https://doi.org/10.1130/G32995.1.